Analysis of the near-side Ridge in high-multiplicity pp collisions at $\sqrt{s} = 13TeV$ via Momentum-Kick model

It's Me,[1*] Mario,[1] Name[2]

[1]Department of Physics, University of Wherever,
An Unknown Address, Wherever, ST 00000, Korea
[2]Another Unknown Address, Palookaville, ST 99999, Korea

[*]To whom correspondence should be addressed; E-mail: jsmith@wherever.edu.

Abstract. Abstract. Abstract. Abstract. Abstract. Abstract. Abstract. Abstract. Abstract. Abstract. Abstract. Abstract. Abstract. Abstract. Abstract. AAAAAAAAAAAAAAAAAAAAAAAAAAAAAAAAAAAAAAAbstract.

Introduction

Ridge structure refers to the shape of 'ridge' that appears at long-range. Previously, Ridge structure was observed in the case of heavy-ion collisions such as PbPb (*1–11*) and AuAu collisions (*12–27*). In this case, they can be understood by collective motion, based on hydrodynamics theory, because it is enough to create high-temperature and high-density environment. And this is the hint of Quark-Gluon Plasma (QGP) state. Recently, however, in the case of high multiplicity of the proton-proton collision, ridge structure is also observed. It was expected that small system could not create such the environment. In this case, the medium doesn't create such the collective motion. Therefore, we will analyze the ridge structure in high multiplicity proton-proton collision at 13TeV, using the Momentum-Kick model (*28–31*).

The Momentum-Kick model is based on pure kinematics between Jet and Medium particles. The Momentum-Kick model assumes that near-side Jet partons transfer their momentum to medium. That model uses the process to explain ridge structure at near-side, which is $\Delta\phi \sim 0$. In this paper, we will analyze the ridge structure using the Momentum-Kick model in high multiplicity proton-proton collision at 13TeV from ALICE, CMS, and ATLAS experiments.

Momentum-Kick Model

The Momentum-Kick model explains the results of experiments at near-side region, through the behavior of near-side jet fragments kicking the medium parton. This model is successfully applying the experimental results in AuAu at 200GeV (*32*) and PbPb at 2.76TeV (*33*), etc. We expect that kinematics behavior is more dominant in the small system than heavy-ion collision. Hence, the Momentum-Kick model will be expected to describe successfully in proton-proton collision at 13TeV in high-multiplicity.

In the Momentum-Kick model, total yield is expressed as follows:

$$\left[\frac{1}{N_{\text{trig}}}\frac{dN_{\text{ch}}}{p_t dp_t d\Delta\eta d\Delta\phi}\right]^{\text{AA}}_{\text{total}} = \left[\frac{2}{3} f_R \langle N_k \rangle \frac{dF}{p_t dp_t d\Delta\eta d\Delta\phi}\right]^{\text{AA}}_{\text{Ridge}} + \left[f_J \frac{dN^{\text{pp}}_{\text{jet}}}{p_t dp_t d\Delta\eta d\Delta\phi}\right]^{\text{AA}}_{\text{Jet}}, \quad (1)$$

which is the sum of ridge and jet fragments. $\Delta\eta$ and $\Delta\phi$ are the difference of η and ϕ between jet and the other particles. f_J is the average survival coefficient of jet fragments, f_R is the average survival factor of ridge particles, and $\langle N_k \rangle$ is the average of kicked partons per-trigger particle.

In the Momentum-Kick model, jet component is written as follow:

$$\frac{dN^{\text{pp}}_{\text{jet}}}{p_t dp_t d\Delta\eta d\Delta\phi} = N_{\text{jet}} \frac{e^{\left[\left(m-\sqrt{m^2+p_t^2}\right)/T_{\text{jet}}\right]}}{T_{\text{jet}}\left(m+T_{\text{jet}}\right)} \times \frac{1}{2\pi\sigma_\phi^2} e^{-\left[(\Delta\phi)^2+(\Delta\eta)^2\right]/2\sigma_\phi^2}, \quad (2)$$

where N_{jet} is the total number of jet particles, T_{jet} is the temperature of jet partons, and σ_ϕ is the

jet cone width, which can be parameterized as:

$$\sigma_\phi = \sigma_{\phi_0} m_a \Big/ \sqrt{m_a^2 + p_T^2}\ . \tag{3}$$

In the equation 2 the exponential term is a Gaussian distribution, which indicates that jet particles are concentrated in the center of the jet cone. Since near-side jet rarely exists in long-range which is $|\Delta\eta| > 1.6$, jet component is not included in this analysis.

The Momentum-Kick model explains ridge component via soft scattering model:

$$\frac{dF}{p_t dp_t d\eta d\phi} = \left[\frac{dF}{p_{ti} dp_{ti} dy_i d\phi_i}\frac{E}{E_i}\right]_{\mathbf{p}_i = \mathbf{p}-\mathbf{q}} \times \sqrt{1 - \frac{m^2}{(m^2 + p_t^2)\cosh^2 y}}. \tag{4}$$

$dF/p_{ti}dp_{ti}dy_i d\phi_i$ is the normalized initial parton distribution, which implies the distribution before freezing out. $\mathbf{p}_i$ is the initial parton momentum, which is the shifted momentum as $\mathbf{p}_i = \mathbf{p} - \mathbf{q}$. $\mathbf{q}$ denotes an average value of kicked momentum. The transverse momentum of initial particles is written as follows:

$$p_{ti}^2 = p_{tf}^2 - \frac{2p_{tf} q \cos(\Delta\phi)}{\cosh(\eta_{\text{jet}})} + \frac{q^2}{\cosh^2 \eta_{\text{jet}}}. \tag{5}$$

Since most of near-side jet is concentrated in the $\Delta\eta, \Delta\phi \sim 0$ region, we set $\eta_{\text{jet}} = 0$. E/E_i insures conservation of energy between initial and final partons. $\sqrt{1 - m^2/(m^2 + p_t^2)\cosh^2 y}$ converts the rapidity into pseudo-rapidity.

The initial parton momentum distribution is expressed as follow:

$$\frac{dF}{p_{ti} dp_{ti} dy_i d\phi_i} = A_{\text{ridge}} (1-x)^a \frac{e^{-\sqrt{m^2 + p_{ti}^2}/T}}{\sqrt{m_d^2 + p_{ti}^2}}. \tag{6}$$

In equation 6, A_{ridge} is the normalization constant satisfying:

$$\int A_{ridge} (1-x)^a \frac{e^{-\sqrt{m^2 + p_{ti}^2}/T}}{\sqrt{m_d^2 + p_{ti}^2}} p_{ti} dp_{ti} dy_i d\phi_i = 1. \tag{7}$$

T is the one of major parameters to explain momentum distribution, indicating the temperature of medium particles. Since pions are expected to take up the majority of partons, we set m as

the pions mass. m_d is a cut-off parameter that prevents divergence at small p_{Ti}. a is a fall-off parameter, which determines the rate of decrease of $1-x$ distribution. m_d and a are set the same as references (*32, 33*) for the general application of the Momentum-Kick model (*32*). Also, x is the light-cone variable written as follow:

$$x = \frac{\sqrt{m^2 + p_{ti}^2}}{m} e^{|y_i| - y_b}, \tag{8}$$

where y_b is the rapidity of the beam defined as $y_b = \cosh^{-1} \sqrt{s_{NN}}/2m_N$. m_N is the mass of beam particles, set as the proton mass.

LHC Detector

We verify our model in ALICE, CMS and ATLAS experiments (*34–36*). The conditions of data analyzed in these experiments are summarized in Table 1.

	ALICE	CMS	ATLAS
$\Delta\eta$ range	$1.6 < \|\Delta\eta\| < 1.8$	$2 < \|\Delta\eta\| < 4$	$2 < \|\Delta\eta\| < 5$
Multiplicity	$0 \sim 0.1\%$	$N > 105$	$N > 90$
p_T range	$1 < p_T < 4$	$0.1 < p_T < 4$	$0.5 < p_T < 5$

Table 1: The ranges of data in ALICE, CMS, and ATLAS experiments (*34–36*)

Moreover, references (*34–36*) used different methods in analyzing their data. In ALICE and CMS analysis, they used Zero Yield At Minimum (ZYAM) method, a traditional experimental analysis method. In this method, the minimum value is set to zero by subtracting. However, ATLAS used the peripheral subtraction method. It takes the ridge component from the experiment data by subtracting the peripheral component, which is low multiplicity pp collisions, to check the flow effect. However, we apply ZYAM method when we use ATLAS experiment data for consistency.

Fitting results

We compare physical parameters in ridge component of Momentum-Kick model at STAR AuAu at 200GeV (*32*), CMS PbPb at 2.76TeV (*33*) and pp at 13TeV, in which ALICE, CMS and ATLAS data are used from reference (*34–36*).

	AuAu 200GeV	PbPb 2.76TeV	pp 13TeV
T (GeV)	0.5	0.6	0.65
q (GeV)	1.0	0.7	0.9
$f_R \langle N_k \rangle$	4	$20.2e^{-\frac{1.395}{\langle p_T^{trig} \rangle}-0.207\langle p_T^{trig} \rangle}$	$0.83 + 0.5{p_T}^2$

Table 2: Physical parameters in ridge component of momentum kick model.

Since T is higher as center of mass energy gets bigger, T becomes higher from 0.5 GeV at AuAu to 0.6 GeV at PbPb. For the same reason, T is 0.65 GeV at pp collision at 13TeV, which is 8.3% higher than PbPb at 2.76TeV.

The medium density from PbPb is expected to be denser than that from AuAu. Since the number of kicks between medium partons is higher, the average of momentum transfer per kick in PbPb is lower than in AuAu, as can be seen, $1.0 \rightarrow 0.7$ GeV in Table 2. However, the medium from pp at 13TeV is expected less dense than that from PbPb, even though the center of mass energy is higher, q becomes higher from 0.7 GeV at PbPb collision to 0.9 GeV at pp collision.

Since the initial parton momentum distribution is normalized, $f_R\langle N_k \rangle$ describe the number of particles, which is reached to the detector. We assumed that particles with high energy can reach the detector more easily. Since the square of pT means energy, we set $f_R\langle N_k \rangle = A + B{p_T}^2$ term (A and B are constants). we also check $f_R\langle N_k \rangle = Ae^{Bp_T}$ form, which is also proportional to p_T. Fig.1 is a graph compared to references (*32, 33*).

The range of p_T^{trig} in PbPb at 2.76TeV is changing while range of p_T^{assoc} kept constant. How-

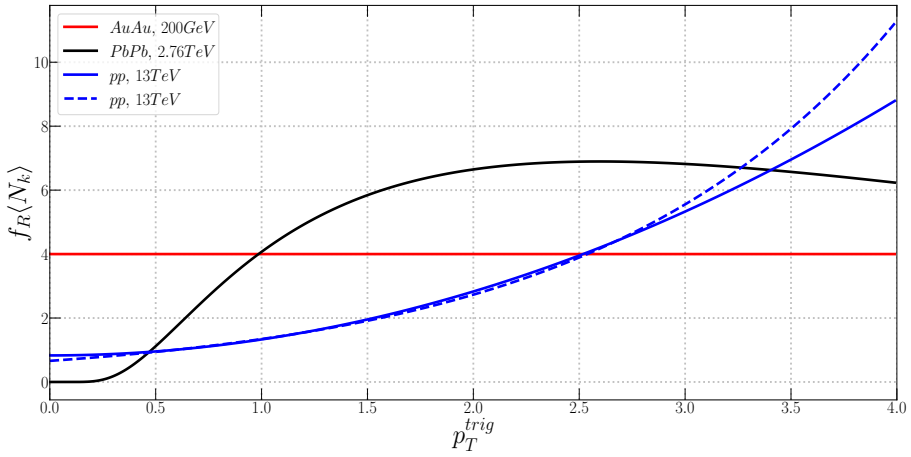

Figure 1: Graphs of $f_R\,\langle N_k\rangle$ fitting results of AuAu 200GeV, PbPb 2.76TeV and pp 13TeV for p_T^{trig}. Dashed line of blue color is $A + Bp_T{}^2$, solid line of blue color is Ae^{Bp_T} term.

ever, in pp at 13TeV, when the range of p_T^{trig} changes, the range of p_T^{assoc} changes together. Hence, it is difficult to compare directly, but it is possible to see trend.

First of all, in the case of AuAu collision at 200GeV, since it has low energy, $f_R\langle N_k\rangle$ doens't have p_T dependence. For this reason, it has the highest at the low p_T. However, in PbPb collision at 2.76TeV, since density of medium is very high, Jet particles transfer their momentum to medium many times. Therefore, many of medium partons, which are received momentum as q, are more likely to reach the detector. As a result, $f_R\langle N_k\rangle$ at PbPb collision has the highest at the mid-range of p_T. In the case of pp collision at 13TeV, since medium density is low, Jet particles kick medium particles a little time. Therefore, because of maximize the effect of survival ratio at high p_T, $f_R\langle N_k\rangle$ is the highest in high p_T. However, since $A + Bp_T{}^2$ and Ae^{Bp_T} have similar trend in $p_T < 4$, we have to check higher p_T range data.

We fit the momentum kick model to the ALICE, CMS, and ATLAS proton-proton Collision 13TeV at high-multiplicity (*34–36*).

In $\Delta\phi$ correlation, we draw Momentum-Kick model result and LHC data. The solid line is the Momentum-Kick model, and circles are the LHC data. And red color is ALICE data and

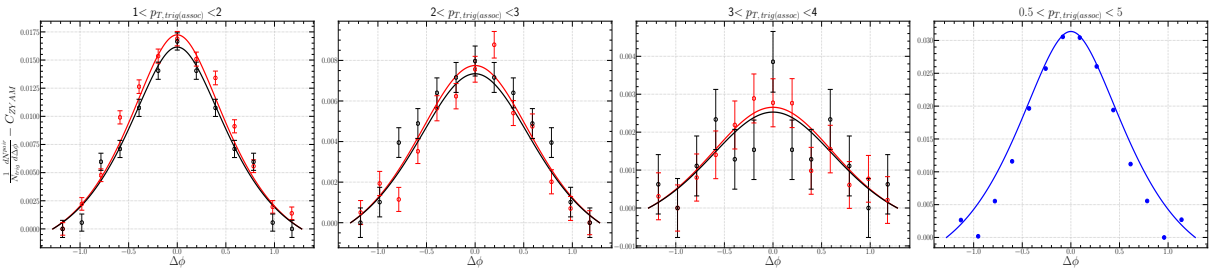

Figure 2: Result for $\Delta\phi$ correlation. All curves are momentum kick model result, plots are experimental data. Red is the result from ALICE, black is from CMS and blue is from ATLAS. For ALICE and CMS data, we draw the case of $1 < p_T < 2, 2 < p_T < 3, 3 < p_T < 4$. And in ATLAS data, we draw for $0.5, p_T < 5$.

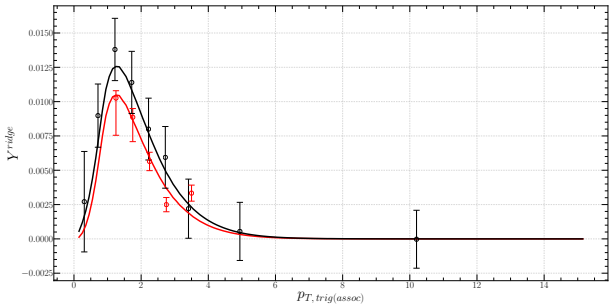

Figure 3: p_T distribution for only ALICE and CMS result. ATLAS couldn't draw because of no result for p_T distribution.

Momentum-Kick model, black is for CMS, and blue is for ATLAS. LHC data is well described via momentum kick model all of p_T range. Since partons are kicked as q by Jet particles, the theoretical ridge yield must show a peak in q. However, since $f_R\langle N_k\rangle$ is exponentially increased for p_T, the position of the peak is moved to an area where the p_T is larger. In this paper, the peak is made around $p_T = 1.2$. Therefore, the momentum kick model can describe well in p_T distribution, too.

Conclusion

We have analyzed the long-range near-side proton-proton collision at $\sqrt{s_{NN}} = 13TeV$in ALICE, CMS and ATLAS data. Since the small system has a less flow effect than heavy-ion

collision, the Momentum-Kick model is expected to be applied well in the high multiplicity pp collision. We apply our model in high multiplicity pp collision at 13TeV data from all 3 collaboration, altogether. As a result, we obtain $T = 0.65\,GeV,\ q = 0.9\,GeV,\ f_R\,\langle N_k\rangle = 0.66e^{0.71p_T}$. Because of higher energy, the medium temperature is 8.3% higher than PbPb collision. Also, because the medium from pp collision has less density than heavy-ion collisions, the total number of kicked medium partons is smaller than PbPb collision at 2.76TeV. Therefore, the average momentum transfer per kicked medium partons is 28.6% higher than PbPb collision at 2.76TeV. Also, we introduce p_T dependence on f_R following reference (*33*). In PbPb at 2.76TeV collision, since high density is created, jet particles kick many of initial medium particles. Therefore, many of final particles, which is middle range of p_T, are created. As a result, $f_R\langle N_k\rangle$ in PbPb collision is the highest in mid-range of p_T. However, in pp collision at 13TeV collision, the survival effect of medium partons is more important than the number of kicked medium partons, because of less density. Therefore, $f_R\langle N_k\rangle$ in pp collision is the highest in high-range of p_T.

Furthermore, we expect the Momentum-Kick model can well describe various energies and multiplicity cuts. Therefore, we will try to explain other diverse data via the Momentum-Kick model.

References

1. V. Khachatryan, *et al.*, *Journal of High Energy Physics* **2010**, 91 (2010).

2. S. Chatrchyan, *et al.*, *Journal of High Energy Physics* **2011**, 76 (2011).

3. S. Chatrchyan, *et al.*, *Physics Letters B* **718**, 795 (2013).

4. S. Chatrchyan, *et al.*, *Physics Letters B* **724**, 213 (2013).

5. S. Chatrchyan, *et al.*, *Journal of High Energy Physics* **2014**, 88 (2014).

6. V. Khachatryan, *et al.*, *Physics Letters B* **742**, 200 (2015).

7. V. Khachatryan, *et al.*, *Phys. Rev. Lett.* **115**, 012301 (2015).

8. V. Khachatryan, *et al.*, *Journal of High Energy Physics* **2016**, 156 (2016).

9. V. Khachatryan, *et al.*, *Physics Letters B* **765**, 193 (2017).

10. B. Abelev, *et al.*, *Physics Letters B* **726**, 164 (2013).

11. J. Adam, *et al.*, *Physics Letters B* **753**, 126 (2016).

12. J. Adams, *et al.*, *Phys. Rev. Lett.* **95**, 152301 (2005).

13. J. Adams, *et al.*, *Phys. Rev. C* **73**, 064907 (2006).

14. W. W. M. Allison, J. H. Cobb, S. J. Holmes, R. C. Fernow, R. B. Palmer, *J. Phys. G* **34**, 679 (2007).

15. A. K. Sisodiya, R. S. Kaushal, D. Parashar, V. S. Bhasin, *J. Phys. G* **34**, 929 (2007).

16. L. Molnar, the STAR Collaboration, *Journal of Physics G: Nuclear and Particle Physics* **34**, S593 (2007).

17. R. S. Longacre, *Int. J. Mod. Phys. E* **16**, 2149 (2007).

18. C. Nattrass, *J. Phys. G* **35**, 104110 (2008).

19. A. Feng, *J. Phys. G* **35**, 104082 (2008).

20. P. K. Netrakanti, *J. Phys. G* **35**, 104010 (2008).

21. O. Barannikova, *J. Phys. G* **35**, 104086 (2008).

22. M. Daugherity, *J. Phys. G* **35**, 104090 (2008).

23. M. van Leeuwen, *Eur. Phys. J. C* **61**, 569 (2009).

24. and F Antinori, *et al.*, *Journal of Physics G: Nuclear and Particle Physics* **37**, 045105 (2010).

25. M. P. McCumber, *J. Phys. G* **35**, 104081 (2008).

26. J. Jia, *J. Phys. G* **35**, 104033 (2008).

27. B. Alver, *et al.*, *J. Phys. G* **35**, 104080 (2008).

28. C.-Y. Wong, *Phys. Rev. C* **76**, 054908 (2007).

29. C.-Y. Wong, *Phys. Rev. C* **78**, 064905 (2008).

30. C.-Y. Wong, *Phys. Rev. C* **80**, 034908 (2009).

31. C.-Y. Wong, *Phys. Rev. C* **84**, 024901 (2011).

32. W. Cheuk-Yin, *Chinese Physics Letters* **25**, 3936 (2008).

33. T. Youn, J.-H. Yoon, *Journal of the Korean Physical Society* **71**, 917 (2017).

34. S. Acharya, *et al.*, *JHEP* **05**, 290 (2021).

35. V. Khachatryan, *et al.*, *Physical Review Letters* **116** (2016).

36. G. Aad, *et al.*, *Phys. Rev. Lett.* **116**, 172301 (2016).